J. Fluid Mech. (1981), *vol.* 112, *pp.* 127–150
Printed in Great Britain

Steady flow in a channel or tube with an accelerating surface velocity. An exact solution to the Navier–Stokes equations with reverse flow

By J. F. BRADY† AND A. ACRIVOS
Department of Chemical Engineering, Stanford University, Stanford, CA 94305

(Received 13 October 1980)

An exact solution to the Navier–Stokes equations for the flow in a channel or tube with an accelerating surface velocity is presented. By means of a similarity transformation the equations of motion are reduced to a single ordinary differential equation for the similarity function which is solved numerically. For the two-dimensional flow in a channel, a single solution is found to exist when the Reynolds number R is less than 310. When R exceeds 310, two additional solutions appear and form a closed branch connecting two different asymptotic states at infinite R. The large R structure of the solutions consists of an inviscid fluid core plus an $O(R^{-\frac{1}{2}})$ thin boundary layer adjacent to the moving wall. Matched-asymptotic-expansion techniques are used to construct asymptotic series that are consistent with each of the numerical solutions.

For the axisymmetric non-swirling flow in a tube, however, the situation is quite different. For $R \leqslant 10{\cdot}25$, two solutions exist which form a closed branch. Beyond 10·25, no similarity solutions exist within the range $10{\cdot}25 < R < 147$. Once R exceeds 147, multiple solutions reappear, which form two closed branches that connect four different asymptotic states at infinite R. The possibility of an axisymmetric flow with swirl is considered, and two sets of swirling solutions are found to exist for all $R > 0$. These solutions, however, do not evolve from the $R = 0$ state nor do they bifurcate from the non-swirling solutions at any finite value of R.

1. Introduction

In this paper we present an exact solution to the steady-state Navier–Stokes equations for the flow inside an infinitely long channel (two dimensions) or tube (axisymmetric) when the surface velocity of the channel or tube grows linearly with the streamwise co-ordinate. As is the case with most such exact solutions, the one to be presented here is of the similarity type, that is, by an assumption as to the form of the flow field, the equations of motion can be reduced to an ordinary differential equation for the similarity function. One of the principal characteristics of this solution is the presence of reverse flow, i.e. the streamwise velocity changes sign in the transverse direction. Like other exact solutions which contain regions of reverse flow, for example, the outflow in a diverging channel – Jeffery–Hamel flow – or the flow between two infinite rotating disks (see Batchelor 1967), the present problem has solution branches which originate and terminate at infinite Reynolds number R and

† Present address: Department of Chemical Engineering, M.I.T., Cambridge, MA 02139.

also has multiple solutions for some range of R. However, an unusual feature of the present problem is that for the flow in a tube there is a range of R within which no solutions exist.

The motivation for this problem arose in studying the flow inside a long slender drop placed in an extensional flow (Brady & Acrivos 1981*b*); as a result, some of the unusual features of the similarity solution are not due to unphysical boundary conditions. The similarity transformation (cf. (2.1) below), in which the velocity field is linearly proportional to the streamwise co-ordinate, has also arisen in a number of other applications. For example, while considering the problem for the steady secondary streaming in a channel or tube with pulsating walls, Secomb (1978) studied the same mathematical problem, but for negative Reynolds numbers. Thus, these two investigations complement one another. The flow in a porous channel or tube with uniform suction or injection at the walls also gives rise to the same ordinary differential equations with, however, different boundary conditions at the surface: $f(1) = 1, f'(1) = 0$ rather than $f(1) = 0$ and $f'(1) = 1$ as in (2.4). This latter problem has already been studied in considerable detail by several authors, most notably Terrill (see Terrill 1964, 1965; Terrill & Thomas 1969; Robinson 1976; Skalak & Wang 1977; as well as others referred to in these papers); and, as we shall show in § 2, these earlier solutions actually form a subset of ours. Thus, although it is a straightforward task to construct the porous-channel (or tube) solutions from those to be presented below, the converse is not true. We shall see, however, that these two sets of solutions do have much in common. Proudman (1960) also investigated the large-Reynolds-number behaviour of the solutions for the porous-channel problem, and, as we shall see, many of his results apply to the case under consideration.

Apart from its physical applications, the flow in a channel with an accelerating surface velocity is an interesting problem to study because it leads to an exact solution and, as such, can give information on the structure of solutions to the Navier–Stokes equations. In addition, since it turns out that the similarity solution also satisfies the boundary-layer equations, we obtain the added bonus of gaining information about these types of flows as well. But, perhaps the greatest interest for studying this flow arises from the presence of a gap in the solutions for the flow inside a tube. We shall see in another publication (Brady & Acrivos 1981*a*) that by resolving this apparent paradox we can gain insight into fluid flows that is of a much more general nature than the specific problem considered here. In this paper, however, we shall only be concerned with presenting the exact solution for the accelerating channel and tube flows.

In § 2 we shall consider the two-dimensional problem for the flow inside a channel. Section 2.1 introduces the similarity transformation that reduces the equations of motion to a single ordinary differential equation. This equation can be solved numerically with ease, and the results are presented in § 2.2. In §§ 2.3 and 2.4 we discuss the asymptotic analysis of the solution for small and for large Reynolds numbers, respectively, and show that asymptotic expansions can be constructed which are consistent with the numerical results.

Section 3 is devoted to the axisymmetric problem for the flow inside a tube, and the discussion parallels that of § 2. The axisymmetric solutions have many features in common with those of the two-dimensional case, with the notable exception that no solutions exist within the range $10{\cdot}25 < R < 147$. In an effort to find solutions in this range of R, we consider, in § 3.3, the possibility of an axisymmetric flow with swirl –

that is, we allow for the presence of a swirling component of motion. It will be seen that, although such solutions do indeed exist, they do not evolve from $R = 0$, nor do they bifurcate from the non-swirling solutions at any finite value of the Reynolds number. Furthermore, we shall see that the swirling solutions have velocity profiles which are quite unrealistic from the physical point of view. Hence, they do not offer a resolution of the paradox concerning the non-existence of similarity solutions without swirl within this range of R.

2. Two-dimensional flow

2.1. *The governing equations*

We wish to examine here the flow inside a two-dimensional, infinite channel which is being driven by a surface velocity proportional to the streamwise co-ordinate. The flow is to be anti-symmetric about the origin $x = 0$; thus, we need only consider the semi-infinite domain $x \geqslant 0$ (see figure 1). The channel has a half-width a, the velocity of the accelerating surface is denoted by Ex and the fluid density and viscosity are ρ and μ respectively.

We seek a solution to the steady-state Navier–Stokes equations in the semi-infinite domain such that the fluid velocity at the surface, $y = a$, is equal to that of the moving boundary $u = Ex$, $v = 0$, where u and v are, respectively, the x and y components of the fluid velocity. We shall restrict our attention to flows that are symmetric about the centre line $y = 0$; thus, $\partial u/\partial y = v = 0$ along this line. Also, we shall render the equations dimensionless by dividing all position co-ordinates by a, all velocities by Ea and the pressure p by μE (a viscous scaling).

It is not difficult to see that the Navier–Stokes equations admit an exact 'similarity solution' for this problem of the form (all variables now being dimensionless)

$$u = xf'(y) \quad \text{and} \quad v = -f(y), \tag{2.1a, b}$$

where the prime denotes differentiation with respect to y. The corresponding pressure is

$$p = p_0(y) + \tfrac{1}{2}\beta x^2, \tag{2.2}$$

where β is a constant and p_0 is a function of y only. Substituting the above into the x-momentum equation leads to

$$f''' - \beta = R\{(f')^2 - ff''\}, \tag{2.3}$$

with the boundary conditions

$$f(0) = f''(0) = 0, \quad f(1) = 0, \quad f'(1) = 1, \tag{2.4}$$

where $R \equiv \rho E a^2/\mu$ is the shear Reynolds number and is the only parameter of the system.

Equation (2.3) is third order with four boundary conditions, the fourth serving to determine the unknown constant β in the expression for the pressure. On the other hand, the y-momentum equation merely yields a relation between p_0 and f, which, being of no interest, shall henceforth be ignored. We also note parenthetically that the similarity function f satisfies a boundary-layer equation in which the transverse co-ordinate y is $O(1)$.

We shall seek all possible solutions to the two-point boundary-value problem for

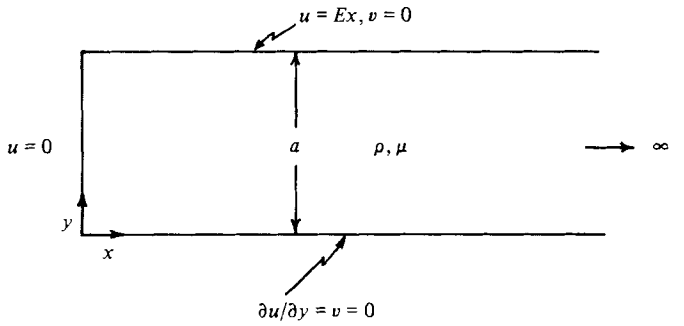

FIGURE 1. Schematic diagram for the flow in a channel with an accelerating surface velocity.

f for all non-negative values of the Reynolds number, $0 \leqslant R < \infty$. Negative Reynolds numbers are permissible and correspond to flows in which the wall of the channel moves inward from infinity to $x = 0$ and have been considered in part by Secomb (1978). (We say in part because Secomb presented only a single solution when $R < 0$ whereas Terrill (1965), and Terrill & Thomas (1969) have shown that the corresponding porous-channel and tube problems with injection have two solutions, and by analogy we would expect the same in this problem.) Furthermore, for our physical application, the surface of the drop only moves in the positive x-direction, and our interest was, therefore, restricted to positive values of R. In contrast, for the porous-channel problem, positive and negative Reynolds numbers correspond to suction and injection respectively and therefore refer to cases of physical interest.

2.2. *The numerical solutions for the similarity function f*

By means of a simple stretching transformation similar to that used by Terrill (1964), it is possible to convert (2.3) into an initial-value problem and, in addition, eliminate the Reynolds number from the equation. We let

$$f = R^{\gamma-1}\phi(\zeta) \quad \text{and} \quad \zeta = R^{\gamma}y, \tag{2.5a, b}$$

where γ is as yet unknown, which when substituted into (2.3) and (2.4) yields

$$\phi''' - \beta^* = (\phi')^2 - \phi\phi'', \tag{2.6}$$

$$\phi(0) = \phi''(0) = 0, \quad \phi(R^{\gamma}) = 0, \quad \phi'(R^{\gamma}) = R^{-1}, \tag{2.7}$$

with

$$\beta^* \equiv \beta/R^{4\gamma-1}. \tag{2.8}$$

The above can now be solved as an initial-value problem for ϕ, with β^* as a parameter. To this end, we set $\phi'(0) = -1, 0$ and $+1$ (the three values for $\phi'(0)$ correspond to the possible directions for the fluid velocity along the centre line), and then vary β^* over the range $-\infty < \beta^* < \infty$ for each choice of $\phi'(0)$. It is easy to see that any other choice for $\phi'(0)$ simply corresponds to changing β^* and would be redundant because β^* is required to cover the entire range of real values. The numerical solution for ϕ proceeds as follows: Given $\phi'(0)$ and β^*, we integrate (2.6) as an initial-value problem until a zero of ϕ is encountered, say at ζ_0. The slope at this point gives directly the Reynolds number, and the value of ζ_0 together with R determine γ. With γ, R and β^*, we can then compute the original function f and the desired parameter β from (2.5) and (2.8). Since our analysis if restricted to positive R, the condition for stopping the marching

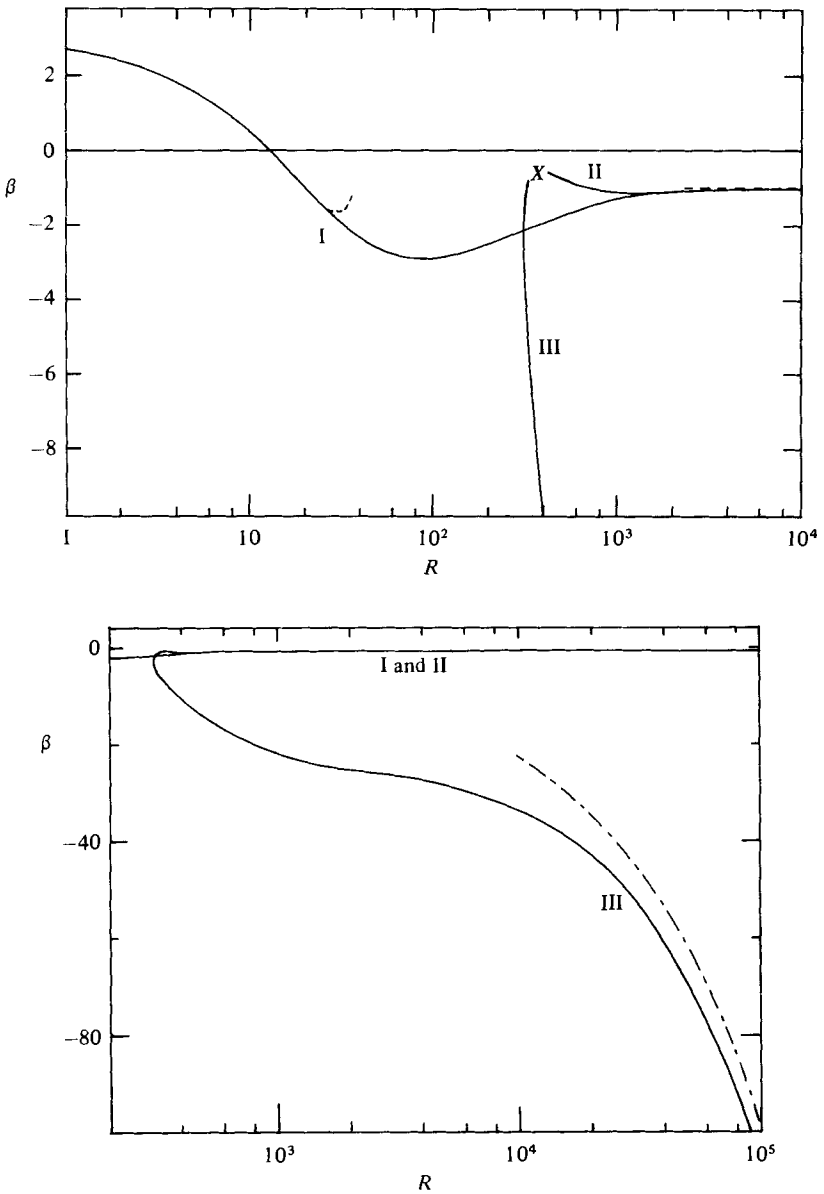

FIGURE 2. (*a*) The pressure coefficient β for the two-dimensional channel flow as a function of the Reynolds number. Three classes of solutions were found, labelled I, II, and III. The dashed curve branching off near $R = 30$ corresponds to the series solution for small R (see §2.3), while that emanating from large R corresponds to the asymptotic solution for $R \to \infty$ (see §2.4(*a*)). (*b*) The high-Reynolds-number behaviour of the pressure coefficient β. The dashed curve corresponds to the asymptotic form of β as $R \to \infty$; the coefficients were determined from the numerical solutions, but the functional dependence on R was determined analytically (see §2.4(*b*)).

scheme is $\phi(\zeta_0) = 0$ *and* $\phi'(\zeta_0) > 0$. Under these conditions, a point must exist within the interval $0 < \zeta < \zeta_0$ where $\phi' = 0$; hence it is clear that all porous-channel solutions, for which $\phi' = 0$ at the wall, are a subset of ours. The integration must, however, cover the entire range of $\zeta > 0$ to allow for the possibility that there are multiple

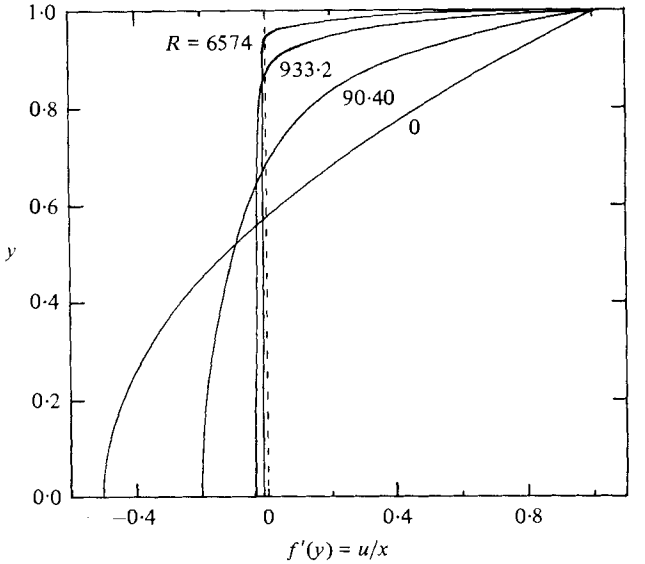

FIGURE 3. Group I longitudinal velocity profiles at $R = 0$, 40, 90, 933·2, and 6574 for the flow in a channel.

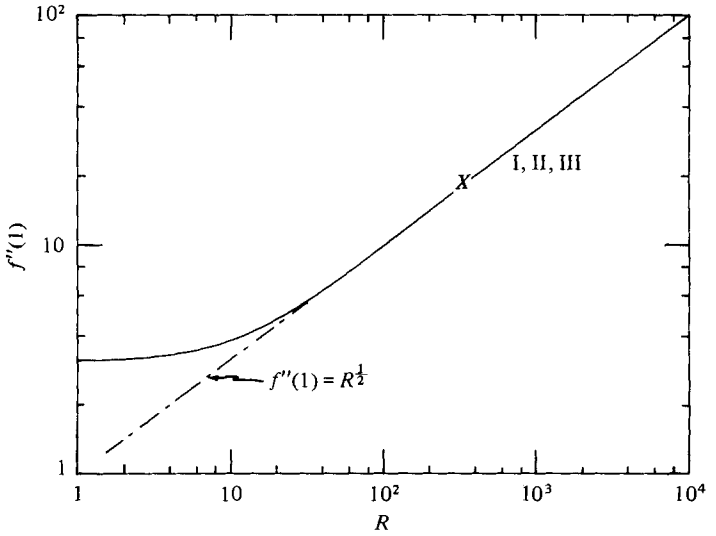

FIGURE 4. $f''(1)$, which is proportional to the shear stress at the channel wall, as a function of R. The dashed curve, $f''(1) = R^{\frac{1}{2}}$, results from the asymptotic analysis as $R \to \infty$ (see §2.4(*b*)).

zeros of ϕ (each with $\phi'(\zeta_0) > 0$). Following the procedure outlined above, (2.6) and (2.7) were integrated using an accurate integration routine.

The results of the numerical integration are most easily presented by referring to figures 2(*a*) and (*b*), where β, the pressure coefficient in (2.2), has been plotted as a function of the Reynolds number R. Clearly, there exists a single solution for

$$0 < R \lesssim 310$$

and three solutions beyond $R \simeq 310$ up to $R = 90400$, the largest Reynolds number for which a numerical solution was computed. These solutions can be conveniently

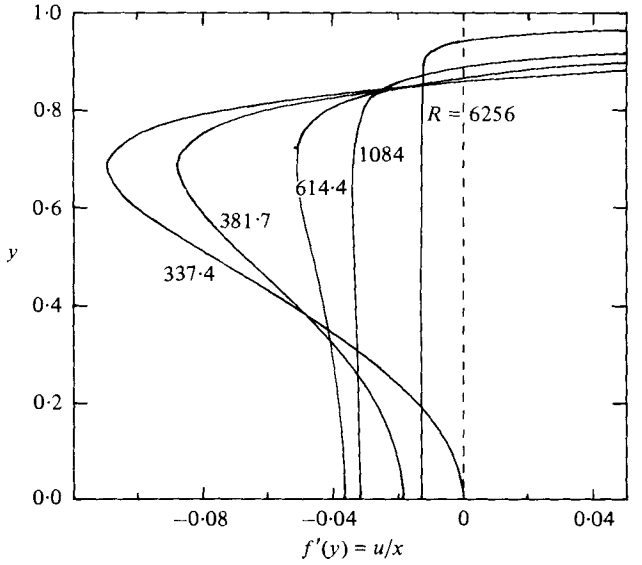

FIGURE 5. Group II longitudinal velocity profiles at R = 6256, 1084, 614·4, 381·7 and 337·4 for the flow in a channel.

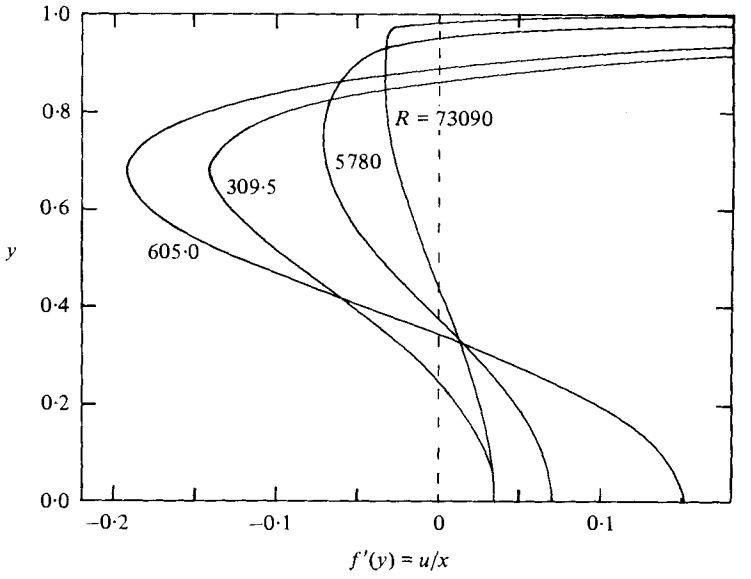

FIGURE 6. Group III longitudinal velocity profiles at R = 309·5, 605·0, 5780 and 73090 for the flow in a channel.

divided into three groups, labelled I, II and III in figure 2(*a*). Figure 2(*b*) shows the large-Reynolds-number behaviour of β, and it is worth noting that all the solutions, but especially those of group III, develop their high-R structure rather slowly, requiring values of R in excess of 10^4 before their asymptotic states are reached. Also, in spite of the fact that an exhaustive search was made to locate solutions having multiple zeros in ϕ, only solutions with single zeros were found.

The group I solutions vary continuously from $R = 0$ with $\beta = 3$ to $R \to \infty$ and $\beta \to -1$. Typical velocity profiles, i.e. $f'(y)$, for these solutions are shown in figure 3. As can be seen, these solutions evolve from the $R = 0$ creeping-flow profile into a flow having the familiar boundary-layer structure, i.e. an inviscid, and in this case uniform, core of strength $O(R^{-\frac{1}{2}})$ plus an $O(R^{-\frac{1}{2}})$ thin boundary layer next to the moving surface. In figure 4 the velocity gradient at the wall $f''(1)$, which is proportional to the shear stress, is seen to increase monotonically with R, becoming $O(R^{\frac{1}{2}})$ at large Reynolds numbers.

In contrast, the group II solutions evolve from the $R \to \infty$ asymptote, where they seem to be identical in all respects to those of group I at the same high Reynolds numbers, and proceed along curve II in the direction of decreasing R until the point marked X in figure 2(a) is reached, where $R = 337{\cdot}4$. Typical velocity profiles for the group II solutions are presented in figure 5. (All of these flows occur at relatively high Reynolds numbers, and only the profiles in the core are shown because, as figure 4 clearly indicates, the boundary layers are virtually identical to those of group I.) As R is decreased, the group II core velocity profiles evolve from being uniform as $R \to \infty$ to having an unusual shape with a maximum in the reverse velocity just beneath the boundary layer. The evolution continues until the point X is reached where the centre-line velocity has increased to zero. (This point corresponds to the $\phi'(0) = 0$ solution of (2.6) and (2.7), there being only one such solution for all β^* since, by a further transformation, β^* can be eliminated from the equation and the boundary conditions.)

The group III solutions, shown in figure 6, are actually a continuation of those of group II beyond the point X. They are distinguished, however, by the presence of a region of fluid moving out towards infinity along the centre line $y = 0$, i.e. the region of reverse flow now lies off the centre line. For these solutions, the pressure coefficient β decreases monotonically with R and becomes $O(R)$ as $R \to \infty$ (see figure 2(b) and the asymptotic analysis of § 2.4) in contrast to the solutions of groups I and II, where β remains $O(1)$. The boundary layer adjacent to the inviscid core still has an $O(R^{-\frac{1}{2}})$ thickness, however, as is clearly shown in figure 4 where the plots of $f''(1)$ against R for the three classes of solutions are all essentially identical.

In spite of some unusual features, the similarity solutions, especially those of group I, exhibit most of the characteristics expected of real fluid motions. Specifically, a solution exists which evolves continuously from the zero-Reynolds-number state as the Reynolds number is increased, ultimately attaining an asymptotic structure where the flow domain is inviscid except for a thin boundary layer. We shall examine next the asymptotic expansion of the solution for small and for large R.

2.3. *The asymptotic analysis for small R*

When the Reynolds number is small, (2.3) can be easily solved using a regular perturbation expansion in R. The solution for zero Reynolds number can be found analytically, as can all higher-order terms. The nth term in the expansion is simply a power series in y of $O(y^{2n-1})$ whose coefficients depend on those from all $n-1$ previous terms. The algebra of calculating these coefficients can be relegated to the computer, and an expansion for β to 29 terms in R was thereby obtained (Brady 1981).

An analysis of this perturbation series by Padé approximants (Van Dyke 1974) revealed the presence of a complex conjugate pair of singularities at $r = 34$ and $\theta = \pm 166{\cdot}5°$, where r and θ are the magnitude and phase angle in the complex plane.

Since these singularities do not lie on the positive real axis in R, they are of no physical significance. No effort was made to extend the radius of convergence of this series by mapping the singularities away. A comparison between this series and the numerical results (cf. figure 2*a*) shows very good agreement almost right up to the singularity.

2.4. *The asymptotic analysis for large R*

Since we have obtained an exact solution to the Navier–Stokes equations which exhibits a boundary-layer structure for large Reynolds numbers, it is of considerable theoretical interest to examine whether the, by now standard, technique of matched asymptotic expansions can yield a representation for the solution that agrees with the numerical results, because there are rather few instances in which asymptotic analyses have been compared with exact solutions. In fact, since the accelerating channel flow involves only a single ordinary differential equation, the asymptotic analysis is algebraically straightforward. This analysis can be conveniently divided into two cases: the first when β remains $O(1)$ as $R \to \infty$, and the second when β scales with the Reynolds number for large R.

2.4(*a*). $\beta = O(1)$ *as* $R \to \infty$

The numerical solutions for both groups I and II show that β remains $O(1)$ for large R and suggest that, as $R \to \infty$, the flow should consist of an inviscid core where the velocity is $O(R^{-\frac{1}{2}})$ plus a conventional $O(R^{-\frac{1}{2}})$ thin boundary layer at the moving surface. It would appear reasonable to expect, therefore, that the high-Reynolds-number structure of the flow could be determined analytically using standard boundary-layer theory.

Let us first examine the flow in the core, which to a first approximation we take to be inviscid. Since the entrainment velocity into the boundary layer is expected to be $O(R^{-\frac{1}{2}})$ – a fact which we shall presently verify – matching between the two regions requires that f be $O(R^{-\frac{1}{2}})$ in the core. Hence, we let

$$f(y) = R^{-\frac{1}{2}} g(y), \tag{2.9}$$

where $g(y)$ is an $O(1)$ function. Substituting the above into (2.3) yields

$$(g')^2 - gg'' = -\beta + R^{-\frac{1}{2}} g''', \tag{2.10}$$

the solution to which must satisfy the boundary conditions on the centre line,

$$g(0) = g''(0) = 0, \tag{2.11}$$

as well as a matching requirement with the boundary-layer solution as $y \to 1$.

Equation (2.10) also arises in the core flow for the porous-channel problem and has been studied by Proudman (1960). Of the possible inviscid solutions presented by Proudman, it is not difficult to see that the leading-order solution to (2.1), denoted here by $g_0(y)$, which satisfies (2.11) is simply

$$g_0(y) = \frac{\alpha}{c^{\frac{1}{2}}} \sin(c^{\frac{1}{2}} y), \tag{2.12}$$

where $\alpha = \pm(-\beta)^{\frac{1}{2}}$ and c is an arbitrary constant which can take on all real, positive and negative, values, including zero. We see also that β must be negative in order for the solution in the core to be real. One should note that, in order to simplify the presentation, we have not expanded β in a series in $R^{-\frac{1}{2}}$, which, in any case, would only add to the expansion some additional terms proportional to $\sin(c^{\frac{1}{2}} y)$.

In view of the boundary conditions at $y = 1$, we must require that $f'(y)$ be $O(1)$ throughout the boundary layer; hence, in this region we have

$$f(y) = R^{-\frac{1}{2}}h(Y) \quad \text{and} \quad y = 1 - R^{-\frac{1}{2}}Y, \tag{2.13a, b}$$

where

$$h''' - hh'' + (h')^2 = -\beta R^{-1}, \tag{2.14}$$

with boundary conditions on h

$$h(0) = 0, \quad h'(0) = -1, \tag{2.15}$$

plus the requirement that h match with the core solution as $Y \to \infty$. As expected, the boundary layer involves a balance between the viscous and inertial terms, the pressure being negligible to leading order.

Matching the derivatives of h and g, i.e. matching u, yields, to leading order, $h'(\infty) = 0$, and it is easy to see that the solution to (2.14), with the right-hand side neglected, which satisfies this condition along with (2.15) is

$$h_0(Y) = -(1 - e^{-Y}). \tag{2.16}$$

This solution appears to have been first noted by Crane (1970) in his study of the boundary-layer flow due to a stretching sheet whose velocity increases linearly with distance.

Matching the entrainment velocity into the boundary layer, $h_0(Y \to \infty) = g_0(y \to 1)$ gives

$$-1 = \frac{\alpha}{c^{\frac{1}{2}}} \sin(c^{\frac{1}{2}}), \tag{2.17}$$

which provides a relation between α and c but does not determine either of them individually. To leading order then we have a continuous spectrum of possible solutions for the flow in the core, all with the same boundary layer. Continuing the expansion in both the core and the boundary layer, one can show (Brady 1981) that the core and boundary-layer solutions can be matched to all orders in $R^{-\frac{1}{2}}$ for any real value of c. The numerical results for both groups I and II show very clearly, however, that $\beta \sim -1$ and $f(y) \sim -R^{-\frac{1}{2}}$ in the core as $R \to \infty$, which are consistent with the asymptotic solutions developed above (cf. (2.12)) if $c = 0$. In this case, (2.12) takes the form

$$g_0(y) = \alpha y,$$

and matching with the boundary-layer solution gives

$$-1 = \alpha = \pm(-\beta)^{\frac{1}{2}},$$

i.e. $\beta = -1$. Also, α being negative indicates that the fluid in the core is returning from infinity. Hence, in order for the asymptotic analysis to agree with the computed results, we need to show that c does indeed equal zero.

To prove that $c = 0$, we follow Proudman (1960) and note, upon differentiating (2.10) twice, that a viscous layer may appear at any y for which $g = g'' = 0$ but $g^{(v)} \neq 0$ – in particular at $y = 0$. This can also be seen from the $O(R^{-\frac{1}{2}})$ correction to the flow in the core,

$$g(y) = \frac{\alpha}{c^{\frac{1}{2}}} \sin c^{\frac{1}{2}}y + R^{-\frac{1}{2}}\left\{B_1(\sin c^{\frac{1}{2}}y - c^{\frac{1}{2}}y \cos c^{\frac{1}{2}}y) - \left[\tfrac{1}{2}c^{\frac{1}{2}} \sin c^{\frac{1}{2}}y \ln|\tan \tfrac{1}{2}c^{\frac{1}{2}}y| - \cos c^{\frac{1}{2}}y \int_0^{c^{\frac{1}{2}}y} \ln|\tan \tfrac{1}{2}\phi| \, d\phi\right]\right\} + o(R^{-\frac{1}{2}}), \tag{2.18}$$

where a logarithmic singularity in g''' appears as $y \to 0$. (Here B_1 is an unknown constant to be found from matching.) One obvious way to remove this singularity and to ensure that g will be an analytic function at $y = 0$, i.e. to ensure that a viscous layer is not necessary, is to set $c = 0$. In this case, the core solution is

$$g = -(-\beta)^{\frac{1}{2}} y$$

to all orders, where β possesses an expansion in powers of $R^{-\frac{1}{2}}$ which enables one to match the core and the boundary-layer solutions.

On the other hand, it is necessary to investigate the structure of this 'internal' viscous layer at $y = 0$ in order to ensure that $c = 0$ is the only possible choice. As shown by Proudman (1960), within this region

$$f(y) = R^{-\frac{3}{4}}\psi(z) \quad \text{and} \quad z = R^{\frac{1}{4}}y, \tag{2.19a, b}$$

where the equation for ψ is

$$\psi''' - \beta = (\psi')^2 - \psi\psi'', \tag{2.20}$$

subject to

$$\psi(0) = \psi''(0) = 0, \tag{2.21}$$

as well as a matching condition as $z \to \infty$. The leading-order solution for ψ is simply

$$\psi_0 = \alpha z, \tag{2.22}$$

which obviously matches with the core. Higher-order terms in the expansion for ψ will be governed by

$$\psi_n''' + \alpha z\psi_n'' - 2\alpha\psi_n' = \Psi_n(z), \tag{2.23}$$

$$\psi_n(0) = \psi_n''(0) = 0, \tag{2.24}$$

where Ψ_n depends only on lower-order solutions and the subscript n refers to the nth term in the expansion for ψ.

The two linearly independent homogeneous solutions of (2.23) for ψ_n', from which the general solution can formally be constructed, are

$$z^2 + \alpha^{-1} \quad \text{and} \quad (z^2 + \alpha^{-1}) \int^z \frac{\exp(-\frac{1}{2}\alpha\xi^2)}{(\xi^2 + \alpha^{-1})^2}\, d\xi; \tag{2.25}$$

from which it is immediately apparent that, as was concluded by Proudman (1960), α must be positive. In other words, an internal viscous layer can exist only if the longitudinal velocity is positive. With this restriction on α, it is then a straightforward matter to show (Brady 1981) that, as $z \to \infty$, the expansion within the internal viscous layer matches with that of the core as $y \to 0$, again for any value of c.

Upon closer examination of (2.17), i.e. the matching requirement between the core solution and that in the boundary layer, it becomes evident that this relation between α and c can be satisfied for positive α only if $c^{\frac{1}{2}} > \pi$. In turn, this implies that the core solution will not be analytic at $y = \pi/c^{\frac{1}{2}}$ – and perhaps, depending on the value of c, at $y = n\pi/c^{\frac{1}{2}}$, $n = 2, 3, \ldots$ as well – and that another internal viscous layer will be required at that point. The longitudinal velocity along $y = \pi/c^{\frac{1}{2}}$ is, however, negative; hence, in view of our earlier analysis, such an internal viscous layer cannot exist.

We can safely conclude, therefore, that the only choice for c that will lead to an asymptotic solution for large R with $\beta = O(1)$ is $c \equiv 0$, in which case the inviscid solution corresponds to an inviscid core with zero vorticity.

This conclusion is in agreement with our numerical results in so far as both the groups I and II solutions have this zero-vorticity core structure for large R. On the other hand, the asymptotic analysis to all finite powers of $R^{-\frac{1}{2}}$ reveals that there is only one asymptotic state with $\beta = O(1)$ as $R \to \infty$, whereas, at any large finite value of R, two numerical solutions were found. To explain this apparent discrepancy, we shall appeal to the work of Terrill (1973) for the corresponding porous-tube problem (cf. § 3) and to that of Robinson (1976) for the porous channel, where it was shown that, when $c = 0$, the asymptotic expansions for the groups I and II solutions differ by exponentially small terms, which, when included in the expansion for f in the core, lead to two distinct solutions. Since our mathematical system is virtually identical to theirs, it is obvious that the same result will apply in the present problem as well. It is therefore not necessary to repeat here their lengthy analysis. Thus, by the inclusion of exponentially small terms, it is possible to determine uniquely two asymptotic expansions for large R that agree with the numerical results. It should be noted, though, that neither Terrill nor Robinson considered the possibility that c could be non-zero, but simply accepted the numerical results as proof that c had to be zero. The proof given above, that all other values of c must be excluded, is far from trivial, however, and should be of interest to those dealing with the development of asymptotic techniques for solving differential equations.

2.4(*b*). $\beta = O(R^{\delta})$ *as* $R \to \infty$

To construct an asymptotic expansion as $R \to \infty$ for the solutions of group III, when β scales with R, is a more complicated undertaking than that presented in the previous section because the functional dependence of β on R is not known *a priori*. (Not having solutions with which to compare his asymptotic results, Proudman (1960) did not consider the possibility that β could scale with R.) Let us assume, therefore, that $\beta = O(R^{\delta})$ as $R \to \infty$, where δ is to be determined. One can show without much effort (Brady 1981) that δ must lie within the range $0 \leqslant \delta \leqslant 1$. This restriction on δ also ensures that, to leading order, the core will be an inviscid region of flow and that the boundary layer will be a conventional, $O(R^{-\frac{1}{2}})$ thin, region. In the analysis that follows, which proceeds along the same lines as § 2.4(*a*), we need only consider the range $0 < \delta \leqslant 1$, the case $\delta \equiv 0$ having been studied previously.

The inviscid core flow involves a balance between the inertial and pressure terms; therefore, we define

$$f = R^{-\frac{1}{2}(1-\delta)}g \quad \text{and} \quad \beta = \beta_0 R^{\delta}, \tag{2.26a, b}$$

where both g and β_0 are $O(1)$. In lieu of (2.10), we have then for g

$$(g')^2 - gg'' = -\beta_0 + R^{-\frac{1}{2}(1+\delta)}g''', \tag{2.27}$$

whose leading-order solution is obviously the same as before, i.e. (2.12), with β replaced by β_0. Similarly, within the boundary layer we have, in place of (2.14),

$$h''' - hh'' + (h')^2 = -\beta_0 R^{-(1-\delta)}. \tag{2.28}$$

Since, clearly, the pressure term will enter to leading order only if $\delta \equiv 1$, we shall consider separately the two cases, $0 < \delta < 1$ and $\delta \equiv 1$.

Case I: $0 < \delta < 1$. When $\delta \neq 1$, f' is of a different order of magnitude in the core

and in the boundary layer, and matching requires that $h_0'(\infty) = 0$. Thus, the leading-order solution for h is the same as (2.16). Matching the functions h and g, i.e. the entrainment velocity v, gives $R^{-\frac{1}{2}}h_0(Y \to \infty) = R^{-\frac{1}{2}(1-\delta)}g_0(y \to 1)$, and hence $g_0(1)$ must be zero, which in turn requires that $c^{\frac{1}{2}} = n\pi$ $(n = 1, 2, 3, \ldots)$. Since $c \neq 0$, an internal viscous layer must be inserted along the centre line to ensure that f is an analytic function giving $\alpha > 0$ as before. Since $c^{\frac{1}{2}} = n\pi$, however, another singularity will appear at $y = 1$ (also others at $y = 1/n, 2/n, 3/n, \ldots$), which requires that the boundary-layer solution give rise to a term proportional to $\ln Y$ as $Y \to \infty$ in order for it to match with the core. The structure of the boundary-layer solution with $e^{-Y} - 1$ as the leading term, however, precludes this possibility (Brady 1981); therefore, we must conclude that δ cannot lie within the range $0 < \delta < 1$.

Case II: $\delta \equiv 1$. With $\delta \equiv 1$, the flow in the core is $O(1)$ as $R \to \infty$, while, within the boundary layer, the pressure term must be retained to leading order. The leading-order solution in the core will be the same as before, i.e. $g_0(y) = (\alpha/c^{\frac{1}{2}})\sin(c^{\frac{1}{2}}y)$, and, since g and h are of different orders, the matching condition gives $g_0(1) = 0$, which again requires that $c^{\frac{1}{2}} = n\pi$, $n = 1, 2, 3, \ldots$. Once more, an internal viscous layer must be introduced along the centre line, giving $\alpha > 0$, and the core expansion will also have singularities in its higher derivatives at $y = 1/n, 2/n, 3/n, \ldots$. When $n > 1$, however, another internal viscous layer will be required about $y = 1/n$ within which the zeroth-order solution in the core has the form $g_0(y) \sim (y - 1/n)\alpha\cos\pi$. The longitudinal velocity along this layer will, however, be negative and hence, as shown previously, an internal viscous layer cannot exist under these conditions. Thus, to have a solution with the assumed structure, n must equal 1 and the boundary-layer solution must give rise to a logarithmic term as $Y \to \infty$. (From his numerical results, Robinson (1976) also concluded that $c^{\frac{1}{2}} = \pi$ for the corresponding set of solutions in the porous-channel problem, but apparently did not carry out an asymptotic analysis of these solutions. As a result his expression for the functional dependence of β on R (cf. his equation (4.11)) is incorrect.) Unfortunately, since the pressure term enters (2.28) to leading order, it is not possible to obtain an exact solution for h_0. Nevertheless, we can show (Brady 1981) that the form of this solution as $Y \to \infty$ satisfies the matching requirements with the core. We can conclude, therefore, that the asymptotic expansion as $R \to \infty$ for the group III solutions must have $\delta = 1$ and $n = 1$, both in perfect agreement with the computed results (cf. figures 2(*b*) and 5). Of course, to complete the analysis we would have to determine α or β_0, but this we were unable to do, owing to the complicated structure of (2.28) which precludes an analytical solution. From the numerical solutions of (2.6) we find $\alpha = 0{\cdot}02$ (or $\beta_0 = 4 \times 10^{-4}$), and the expansion for β is of the form $\beta = 4{\cdot}00 \times 10^{-4}R\{1 + (4{\cdot}64 \times 10^2)R^{-\frac{1}{2}} + O(R^{-1}\ln R, R^{-1})\}$.

We have seen then that the asymptotic analysis as $R \to \infty$ leads to solutions which are completely consistent with the numerical results both when $\beta = O(1)$ and when $\beta = O(R)$. The structure of the asymptotic solution is, however, somewhat different from what one would normally have expected. Specifically, exponentially small terms play a key role in distinguishing between the solutions of groups I and II, and the group III solutions require the existence of an $O(R^{-\frac{1}{4}})$ thick viscous layer at $y = 0$. Also, in spite of the fact that the leading-order core solutions were non-unique, the application of matched-asymptotic-expansion techniques allowed us to determine unique solutions when $\beta = O(1)$ and to find both δ and n when β scales with the Reynolds number.

3. Axisymmetric flow

3.1. *The governing equations and numerical results*

This section deals with the similarity solution for the flow in a tube with an accelerating surface velocity – the axisymmetric analogue of the problem considered in § 2. The two problems are very much alike; hence, our treatment here will be quite brief. We consider the same flow as depicted in figure 1 with y replaced by the radial variable r. Scaling the equations in the same manner as before, it is easy to see that the Navier–Stokes equations admit an exact similarity solution of the form

$$u = xf'(r)/r \quad \text{and} \quad v = -f(r)/r, \tag{3.1}$$

where the prime denotes differentiation with respect to r. The pressure distribution accompanying this velocity field has the same form as (2.2). With β and R being the same as in the two-dimensional case, the differential equation satisfied by f is

$$\frac{1}{r}\frac{d}{dr}r\frac{d}{dr}\left(\frac{f'}{r}\right) - \beta = R\left\{\left(\frac{f'}{r}\right)^2 - \frac{f}{r}\left(\frac{f''}{r} - \frac{f'}{r^2}\right)\right\}, \tag{3.2}$$

with

$$f(0) = f'(0) = 0, \quad f(1) = 0, \quad f'(1) = 1. \tag{3.3}$$

By means of the stretching transformation $f(r) = R^{-1}\phi(\zeta)$, $\zeta = R^{\gamma}r$ and $\beta^* = \beta/R^{4\gamma-1}$, (3.2) was converted to an initial-value problem and numerically solved using the same integration scheme as before, i.e. $\phi''(0)$ was set equal to $-1, 0$ and $+1$, and β^* covered the range $-\infty < \beta^* < \infty$. The results of the numerical integration are shown in figure 7 where β has been plotted as a function of R. Unlike the two-dimensional flow, there are two solutions for $0 \leqslant R < 10{\cdot}25$, followed by a gap in Reynolds number, $10{\cdot}25 < R < 147$, within which no solutions exist, and then multiple solutions reappear for Reynolds numbers greater than 147. The solutions can be conveniently divided into four groups which are labelled I, II, III and IV in figure 7.

The group I solutions, whose longitudinal velocity profiles, i.e. $f'(r)/r$, are shown in figure 8, begin with the $R = 0$ solution for which $\beta = 8$ and evolve in a continuous manner as the Reynolds number is increased until $R = 10{\cdot}25$. Rather than continuing beyond this point, the solutions proceed back along the lower portion of curve I, now as the Reynolds number decreases. The velocity profiles along this section of curve I have rather curious shapes with a maximum in the velocity just beneath the moving surface. As the Reynolds number approaches zero, the flow attains an asymptotic state in which both the pressure and the velocity are $O(R^{-1})$. (The numerical solutions give $\beta \sim -35R^{-1}$ and $f''(0) \sim -35R^{-1}$ as $R \to 0$.) If β and f are scaled with R^{-1}, we see that the asymptotic form of these solutions satisfies the full equation of motion (3.2), but with homogeneous boundary conditions (to leading order). Thus, in some sense, they represent an eigensolution of (3.2). Corrections to this asymptotic state can be obtained by a regular perturbation expansion in R, as can the other branch of curve I emanating from $\beta = 8$. In contrast to the two-dimensional flow, however, there are no solutions which evolve continuously from $R = 0$ to $R \to \infty$.

The lack of solutions beyond $R = 10{\cdot}25$ is quite puzzling because, as seen by the shear-stress plot of figure 9 ($f''(1) - 1$ is proportional to the shear stress at the wall), nothing particularly unusual seems to occur at this point. Indeed, the shear stress at the wall does not even vanish at this Reynolds number as it does for the corresponding porous-tube problem (see Terrill & Thomas 1969). In order to understand more fully

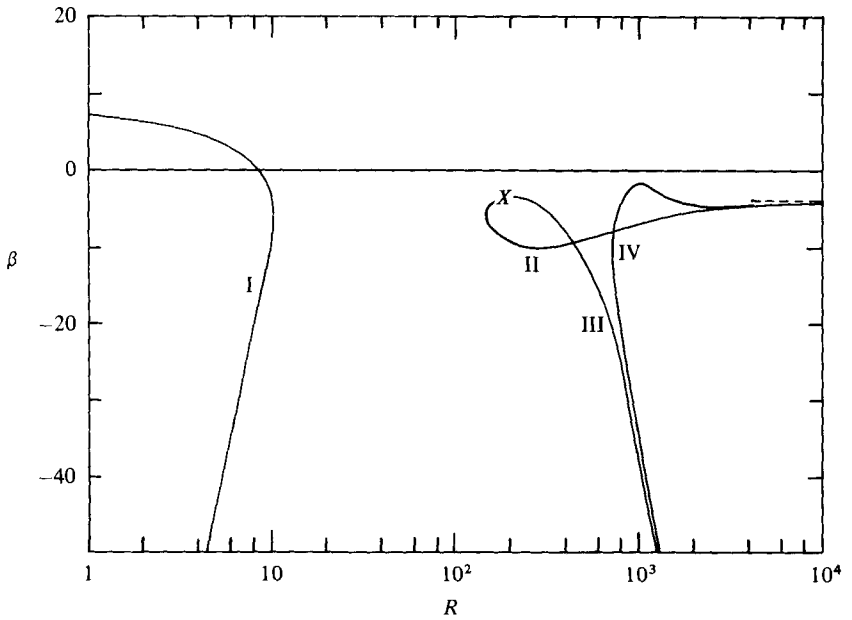

FIGURE 7. The pressure coefficient β for the axisymmetric flow in a tube as a function of the Reynolds number. Four classes of solutions were found, labelled I, II, III and IV.

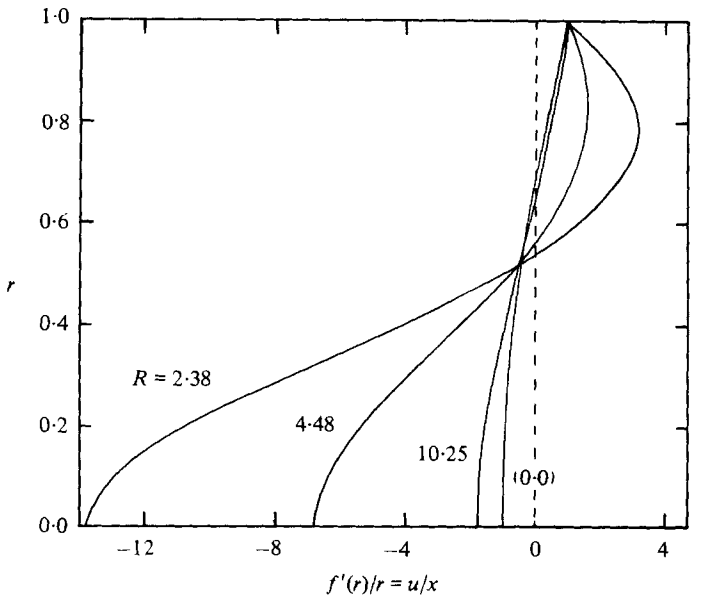

FIGURE 8. Group I longitudinal velocity profiles at $R = 0$, 10·25, 4·48 and 2·38 for the flow in a tube.

the nature of this 'singularity' at $R = 10{\cdot}25$, (3.2) was also solved by means of a regular perturbation expansion in R in the same manner as for the two-dimensional problem. When the resulting series for β – whose coefficients were computed up to $O(R^{35})$ – was examined by means of a Domb–Sykes plot and Neville table (Van Dyke 1974, 1978), it was found to possess a square-root singularity on the positive real axis

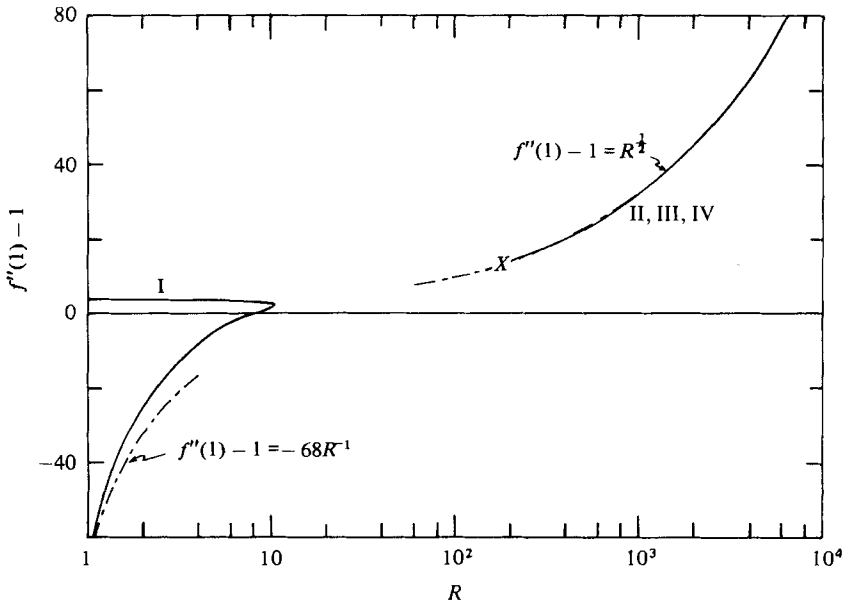

FIGURE 9. $f''(1)-1$, which is proportional to the shear stress at the tube wall, as a function of R. The dashed curve $f''(1)-1 = R^{\frac{1}{2}}$ results from the asymptotic analysis as $R \to \infty$ (see §3.2), while the curve $f''(1)-1 = -68R^{-1}$ was determined from the numerical solutions of Group I as $R \to 0$.

in Reynolds number at $R = 10{\cdot}25$. The presence of such a singularity is a further indication that the similarity solution no longer provides a valid description of the flow when R exceeds 10·25.

Beyond the gap in Reynolds number, quite a variety of solutions appear. The group II solutions, shown in figure 10, are in many ways similar to the group II solutions for the two-dimensional flow (cf. figure 5). They originate from a large R solution, which has an inviscid core with velocity $O(R^{-\frac{1}{2}})$ surrounded by a thin, $O(R^{-\frac{1}{2}})$, boundary layer, and vary continuously along curve II as the Reynolds number is decreased until the point X at $R = 186{\cdot}0$ is reached. As before, this point corresponds to the Reynolds number at which the centre-line velocity has increased to zero. Similarly, the group III solutions, shown in figure 11, which are a continuation of the group II solutions beyond the point X, have the same structure as the group III solutions in the two-dimensional flow. Moreover, as seen in figure 9, where $f''(1)-1$ has been plotted as a function of R, a conventional, $O(R^{-\frac{1}{2}})$ thin, boundary layer forms adjacent to surface for both groups of solutions.

The velocity profiles for the group IV solutions are shown in figure 12. For large Reynolds numbers, when β is $O(1)$, these solutions are of the same form as the group I solutions for the two-dimensional flow – that is, the flow consists of an inviscid core of zero vorticity surrounded by a conventional boundary layer. As the Reynolds number is decreased from infinity, however, these solutions develop velocity profiles in which the fluid at the centre line and just beneath the boundary layer moves more rapidly than the fluid midway between the centre line and the wall. Once the Reynolds number has been decreased below approximately 900, the solutions develop a region of flow midway between the axis and the wall where the fluid moves in the positive

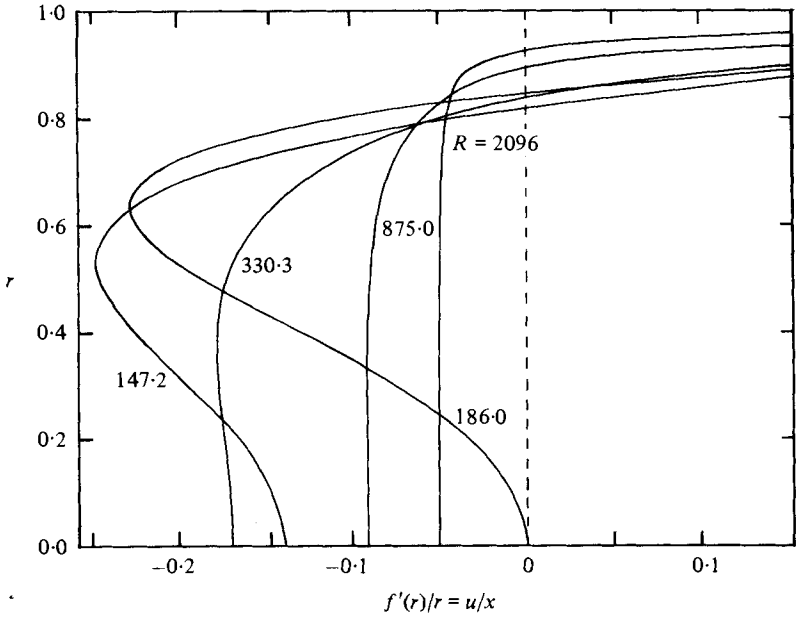

FIGURE 10. Group II longitudinal velocity profiles at R = 2096, 875·0, 330·3, 147·2 and 186·0 for the flow in a tube.

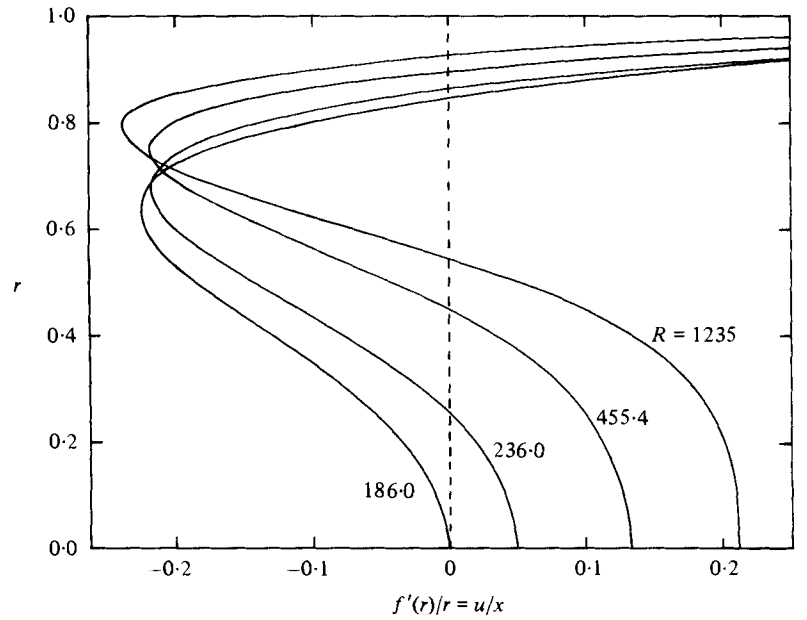

FIGURE 11. Group III longitudinal velocity profiles at R = 186·0, 236·0, 455·4 and 1235 for the flow in a tube.

direction. As the Reynolds number is increased again, there are now three different regions of flow in the core, and, of course, the same boundary layer at the surface. Like the group III solutions, β now scales with the Reynolds number as $R \to \infty$.

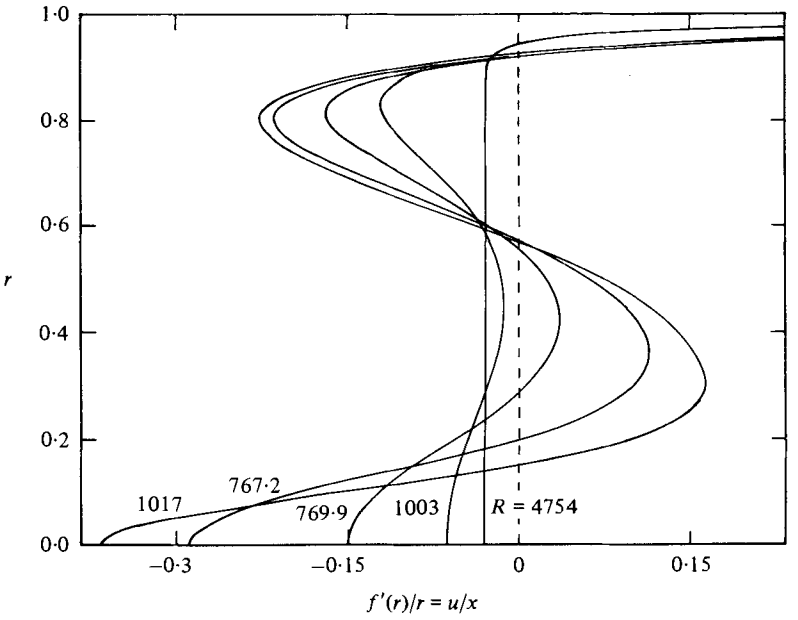

FIGURE 12. Group IV longitudinal velocity profiles at $R = 4754$, 1003, 769·9, 762·2 and 1017 for the flow in a tube.

3.2. *Asymptotic analysis as* $R \to \infty$

As might be expected, the asymptotic analysis for the axisymmetric flow is quite similar to that for the two-dimensional flow. There are, however, some important differences, most notably the fact that there are four solutions as $R \to \infty$ in axisymmetric flow, but only three in two dimensions. It is of interest, therefore, to present the asymptotic analysis for the axisymmetric flow in order to see how these differences arise. First of all, if we introduce the change of variables $\eta = r^2$ in (3.2) and define a new similarity function $\bar{f} = 2f$, then the equation for $\bar{f}$ becomes

$$\eta\bar{f}''' + \bar{f}'' - \tfrac{1}{4}\beta = \tfrac{1}{4}R\{(\bar{f}')^2 - \bar{f}\bar{f}''\}, \tag{3.4}$$

$$\bar{f}(0) = 0, \quad \lim_{\eta \to 0} \eta^{\frac{1}{2}}\bar{f}'' = 0, \quad \bar{f}(1) = 0, \quad \bar{f}'(1) = 1, \tag{3.5}$$

where β and R are the same as in (3.2). Although the viscous terms and one boundary condition at $\eta = 0$ are different, the inertial terms are the same as in the two-dimensional case (cf. (2.3)); hence, much of the previous analysis can be carried over unchanged.

Let us consider the case when β remains $O(1)$ as $R \to \infty$. By using the same scalings as in the two-dimensional flow, with the exception that R is replaced by $\frac{1}{4}R$, i.e. $\bar{f} = (\frac{1}{4}R)^{-\frac{1}{2}}g$ in the core and $\bar{f} = (\frac{1}{4}R)^{-\frac{1}{2}}h(Y)$, $Y = (\frac{1}{4}R)^{+\frac{1}{2}}(1-\eta)$ in the boundary layer, it is easy to see that the leading-order solutions in both regions are the same as in the two-dimensional case (cf. (2.12) and (2.16)). It might be anticipated that by differentiating (3.4) a sufficient number of times we could show the need for a viscous layer at $\eta = 0$ and simply repeat the analysis of § 2.4. As we shall now show, however, this argument is not sufficient to guarantee the existence of a viscous layer.

Although governed by the same leading-order solution as in the two-dimensional case, the corrections to (3.4) are different; thus, for the $O(R^{-\frac{1}{2}})$ correction we have

$$g = \frac{\alpha}{c^{\frac{1}{2}}}\sin c^{\frac{1}{2}}\eta + (R/4)^{-\frac{1}{2}}\left\{\tfrac{3}{2}\cos c^{\frac{1}{2}}\eta + B_1(\sin c^{\frac{1}{2}}\eta - c^{\frac{1}{2}}\eta\cos c^{\frac{1}{2}}\eta)\right.$$
$$-\frac{1}{2}\left[3 + c^{\frac{1}{2}}\eta\sin c^{\frac{1}{2}}\eta\ln|\tan\tfrac{1}{2}c^{\frac{1}{2}}\eta|\right.$$
$$-(\sin c^{\frac{1}{2}}\eta - c^{\frac{1}{2}}\eta\cos c^{\frac{1}{2}}\eta)\int_0^{c^{\frac{1}{2}}\eta}\ln|\tan\tfrac{1}{2}\phi|\,d\phi$$
$$\left.\left.-2\cos c^{\frac{1}{2}}\eta\int_0^{c^{\frac{1}{2}}\eta}\phi\ln|\tan\tfrac{1}{2}\phi|\,d\phi\right]\right\} + o((R/4)^{-\frac{1}{2}}), \tag{3.6}$$

where $\alpha = \pm(-\frac{1}{4}\beta)^{\frac{1}{2}}$ and B_1 is an unknown constant, which should be compared with the corresponding expression (2.18). The appearance of the logarithmic terms in (3.6) would suggest that the core solution as developed will have singularities at $\eta = 0$ as well as at $c^{\frac{1}{2}}\eta = n\pi$, with n being a positive integer. In fact, it can be shown that, in contrast to the corresponding two-dimensional solution (2.18), the above expression for g *is* analytic at $\eta = 0$ (but not for all $\eta \neq 0$), and it is not difficult to show that higher-order corrections will similarly be analytic along the tube axis. Therefore, a viscous layer is not necessary along $\eta = 0$, and it is not possible to conclude that $c = 0$ by repeating the arguments used earlier in the two-dimensional case. Recall that in the two-dimensional flow, y can take on both positive and negative values, while, in the axisymmetric flow, η can only be positive; hence, the different natures of the equations on the centre line. From (2.17), the matching condition between the core and the boundary-layer expansions, we can, however, restrict α to the range $-\infty < \alpha \leqslant -1$ by requiring that $0 \leqslant c^{\frac{1}{2}} < \pi$ which would render the core solution analytic in $0 \leqslant \eta \leqslant 1$.

Unfortunately, in spite of many attempts, we have not been able to proceed further and prove uniqueness for the $\beta = O(1)$ solutions of groups I and IV. It is conceivable, of course, that if the expansions in the core and the boundary layer were carried out to higher order, a condition would emerge which would prevent α from lying within its acceptable range; however, a resolution of this intriguing question remains to be worked out.

As before, the $c = 0$ solution gives

$$g = -(-\tfrac{1}{4}\beta)^{\frac{1}{2}}\eta$$

for all R, which, when matched to the boundary-layer solution, leads to $\beta = -4$, in agreement with the numerical results. Of course, as in the two-dimensional case, the solutions for groups II and IV differ in their asymptotic expansions by exponentially small terms as was shown by Terrill (1973) for the corresponding porous-tube problem.

As expected, the asymptotic analysis of the solutions when β scales with R as $R \to \infty$ has many features in common with its two-dimensional counterpart treated in § 2.4 (*b*). In fact, by repeating the analysis of that section, it is easy to show that the axisymmetric solutions corresponding to group III have a structure virtually identical to the two-dimensional group III solutions except, of course, for the absence of an 'internal viscous layer' along the axis. Thus, for the group III solutions we have

$$\beta = \beta_0 R, \quad g_0(\eta) = \frac{\alpha}{n\pi}\sin(n\pi\eta), \quad n = 1, \tag{3.7}$$

and the boundary-layer equation at the surface has the pressure gradient included to leading order as before.

The numerical results for both the shear stress at the wall (figure 9) and β (figure 7) indicate that the asymptotic structure of the group III and the group IV solutions will be very similar. In fact, the group IV longitudinal velocity profiles in the core (see figure 12) can be described by (3.7) with $n = 2$. In § 2.4(*b*) we showed that the two-dimensional core expansion has singularities at $y = 1/n$ that cannot be removed when $n > 1$ by the insertion of an internal viscous layer at that point because the axial velocity would then be $-\alpha$ to leading order and therefore negative – recall that, in the two-dimensional case, the presence of an internal viscous layer along $y = 0$ requires that α be positive. For axisymmetric flows, however, α is not restricted to being positive, and we shall now show that it is possible to have a solution with $n = 2$.

The boundary layer at the surface $\eta = 1$ is the same as in the two-dimensional flow; thus, we must require $h'(\infty)$ $(= -g'(1))$ to be positive in order for the boundary layer to give rise to the necessary logarithmic term. From (3.7) we see that $h'(\infty) = -\alpha(-1)^n$, which is indeed positive for $n = 2$ if $\alpha < 0$. With $n = 2$, the expansion for the core solution will have a singularity at $\eta = \frac{1}{2}$, but from (3.7) we see that $g' \sim -\alpha$ as $\eta \to \frac{1}{2}$, which is positive when $\alpha < 0$. Therefore, an internal viscous layer can be inserted at $\eta = \frac{1}{2}$ that will remove the singularity. In general, then, the expansion in the core can have one of two structures: $n = 1$ if $\alpha > 0$ and $n = 2$ if $\alpha < 0$, both with the same boundary layer at the surface. (It is not difficult to see that $n > 3$ is unacceptable regardless of the sign of α, for this would result in multiple singularities in $0 < \eta < 1$, all of which could not be removed by introducing internal viscous layers.) Hence, we see that the absence of a singularity at $\eta = 0$ in the core solutions for the axisymmetric flow is of crucial importance because it allows us to have solutions with both positive and negative α's. As in the two-dimensional case, the actual value of α or β_0 cannot be easily found. Thus, although we have been able to construct asymptotic expansions which are consistent with each of the numerical solutions, both are still partially incomplete.

3.3. *Axisymmetric flow with swirl*

As we have already remarked several times, the most striking feature of the axisymmetric solutions is that they exist only outside the Reynolds number range

$$10{\cdot}25 < R < 147.$$

One possible way of removing this gap in the solutions is to postulate that an axisymmetric flow with a swirling component of motion exists when the Reynolds number exceeds 10·25. It is not difficult to see that the Navier–Stokes equations admit an exact similarity solution of the following form

$$u = xf'(r)/r, \quad v = -f'(r)/r \quad \text{and} \quad w = xs(r), \qquad (3.8a, b, c)$$

where w is the angular component of the fluid velocity. The pressure distribution is now

$$p = p_0(r) + \frac{1}{2}\left[\beta + 2R\int_0^r \frac{s^2(\xi)}{\xi}\,d\xi\right]x^2, \qquad (3.9)$$

the $O(x^2)$ term of which is seen to vary radially as a result of the swirling motion. The equation for f is the same as before, i.e. (3.2) with β replaced by

$$\beta_s(r) \equiv \beta + 2R\int_0^r \frac{s^2(\xi)}{\xi}\,d\xi,$$

while the equation for s is

$$\left(\frac{1}{r}\frac{d}{dr}r\frac{d}{dr}-\frac{1}{r^2}\right)s = R\left\{\frac{f'}{r}s-\frac{f}{r}s'-\frac{fs}{r^2}\right\}, \tag{3.10}$$

$$s(0) = 0, \quad s(1) = 0. \tag{3.11}$$

Terrill & Thomas (1973) also computed swirling flows for the corresponding porous-tube problem, and their solutions, again being a subset of ours, have the same general features as those to be presented below.

For the numerical computations f was stretched in the same manner as before – $f(r) = R^{-1}\phi(\zeta)$, $\zeta = R^{\gamma}r$ and $\beta^* = \beta/R^{4\gamma-1}$ – while s was stretched with $R^{2\gamma-1}$, which had the effect of converting the equation for f into an initial-value problem and of eliminating the Reynolds number from both equations. Unfortunately, the equations for f and s cannot be simultaneously converted into initial-value problems, and therefore Newton's method was used to iterate on $s'(0)$. We should also note that when $R \equiv 0$ the only solution with s of order unity is $s = 0$; thus, flows with swirling motion cannot evolve from the zero-Reynolds-number state. The results for the numerical computations are shown in figure 13, where the coefficient $\beta_s(1)$ of the x^2 term in the expression for the pressure (see (3.9)), evaluated at the surface $r = 1$, has been plotted against the Reynolds number. For comparison, β for the axisymmetric solutions without swirl is also shown in figure 13. Two sets of swirling solutions, labelled V and VI in figure 13, were found to exist, and we see that swirling solutions do indeed exist within the range $10{\cdot}25 < R < 147$.†

Figures 14 and 15 depict, respectively, the longitudinal and swirling components of velocity for the group V solutions. It is seen that $s \to 0$ as $R \to \infty$ and that the swirling solutions become identical to those of group II without swirl. In fact, since f is $O(R^{-\frac{1}{2}})$ as $R \to \infty$ (corresponding to the group II solutions) and (3.10) is linear in s, we see that the swirling component of motion can only arise from the exponentially small terms that are present in the large-Reynolds-number expansion for f. As the Reynolds number is decreased, the axial component of velocity develops profiles which are very similar to those of groups II and III (cf. figures 10 and 11), without of course, the boundary layer at the surface. At the same time, the swirling motion grows in strength and reaches its maximum midway between the centre line and the wall. As $R \to 0$, both f and s become of $O(R^{-1})$, and, remarkably, the swirling solutions have the same mathematical structure as the group I solutions with negative β. Figures 16 and 17 show the longitudinal and swirling components of velocity for the group VI solutions. In this case, the solutions evolve from the group IV solutions as $R \to \infty$, and the axial velocity profiles are seen to be very similar to those of group IV (cf. figure 12). Although these solutions are very interesting as an exact solution to the Navier–Stokes equations, they do not evolve from the $R = 0$ state nor bifurcate from the non-swirling solutions at any finite value of R; thus, it is difficult to imagine that they would represent a real flow.

We have seen in this paper that the similarity solution for the flow inside an infinite channel or tube with an accelerating surface velocity has many interesting, and some

† Although we did not compute swirling solutions for Reynolds numbers less than 30, Terrill & Thomas (1973) showed, for the corresponding porous tube problem, that two sets of swirling solutions exists for all $R > 0$; hence, we expect the same to be true in this case.

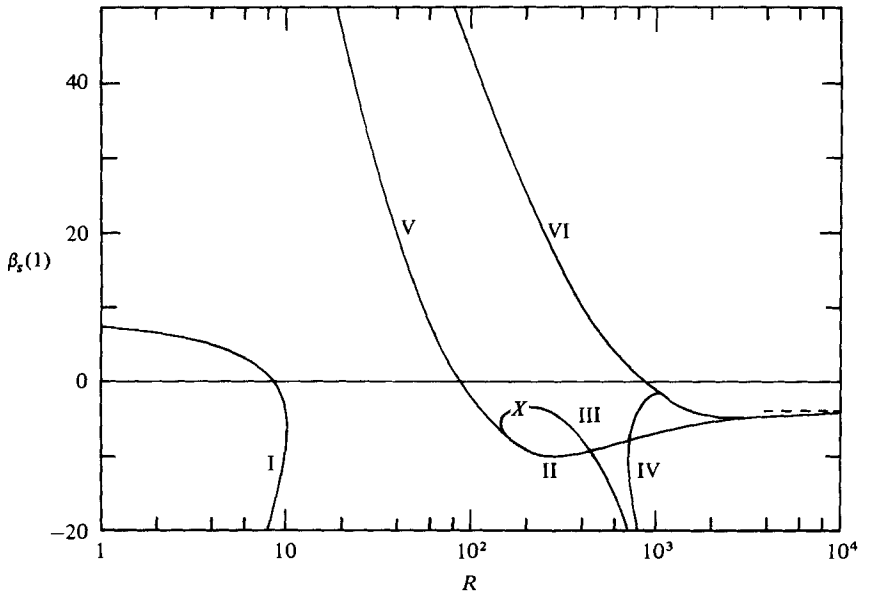

FIGURE 13. The pressure coefficient $\beta_s(1)$ evaluated at $r = 1$ for the axisymmetric swirling flow in a tube as a function of the Reynolds number. Two classes of solutions were found, labelled V and VI. For comparison, β for the axisymmetric flow without swirl is also shown.

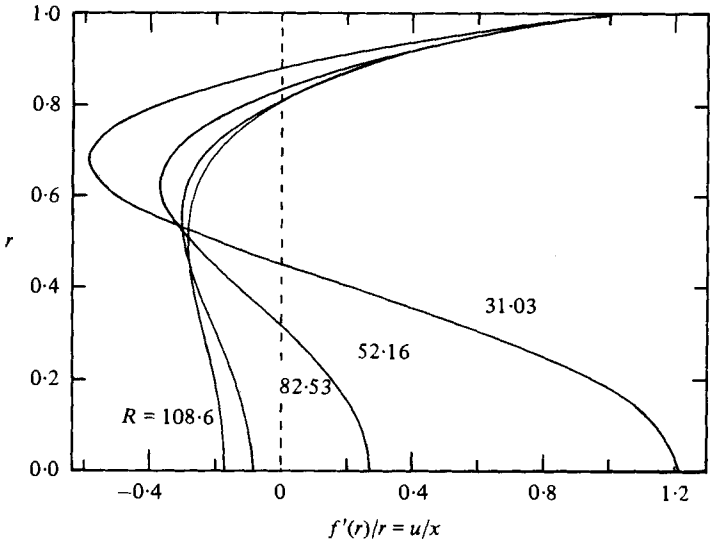

FIGURE 14. Group V longitudinal velocity profiles at $R = 108{\cdot}6$, 82·53, 52·16 and 31·03 for the axisymmetric flow in a tube with swirl.

very unusual, features. In general, the similarity solution has many of the characteristics expected of real fluid motions, for example, as $R \to \infty$, a conventional $O(R^{-\frac{1}{2}})$ thin boundary layer forms adjacent to the moving surface. Also, in the two-dimensional flow, a well-behaved set of solutions exists for all values of R, which allows the flow in a channel to evolve continuously with increasing Reynolds numbers. In the axisymmetric case, however, the situation is quite different, as there is a range of Reynolds

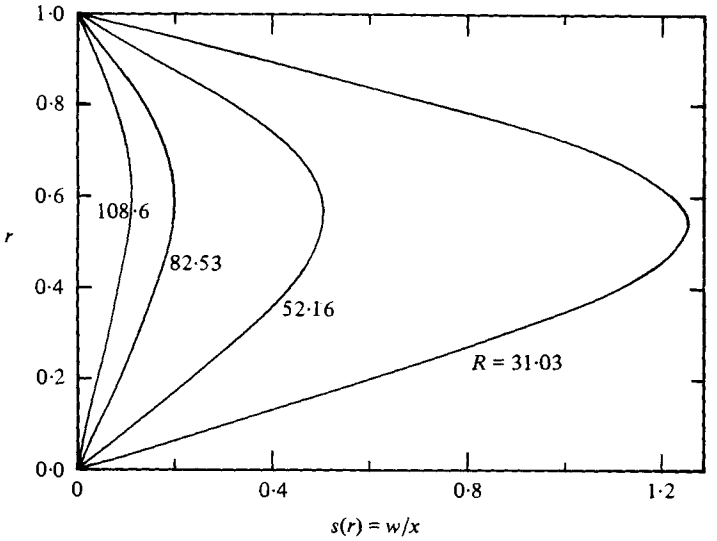

FIGURE 15. Group V swirling velocity profiles at $R = 108{\cdot}6$, $82{\cdot}53$, $52{\cdot}16$ and $31{\cdot}03$ for the axisymmetric flow in a tube with swirl.

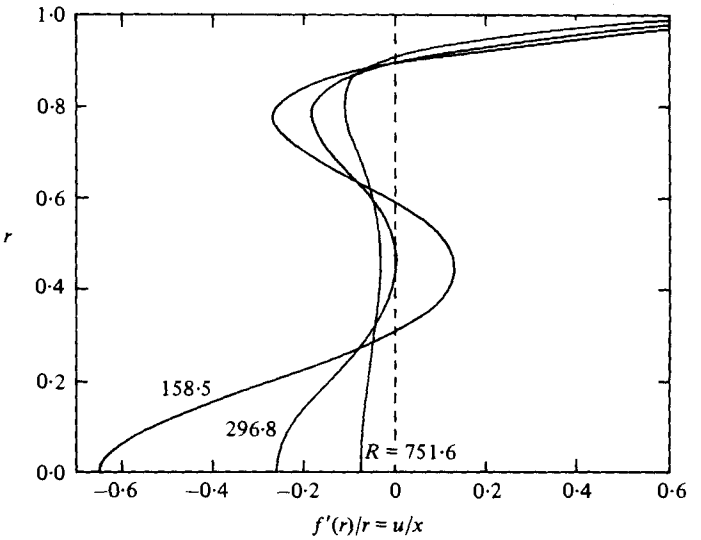

FIGURE 16. Group VI longitudinal velocity profiles at $R = 751{\cdot}6$, $296{\cdot}8$ and $158{\cdot}5$ for the axisymmetric flow in a tube with swirl.

number within which non-swirling similarity solutions do not exist. This disappearance of such similarity solutions at $R = 10{\cdot}25$ raises an important question concerning the structure of the flow in a very long tube as the Reynolds number is increased from zero to $10{\cdot}25$ and then beyond. In a subsequent paper (Brady & Acrivos 1981*a*) we shall address this question and show how to construct solutions for such systems which evolve continuously as the Reynolds number is increased to well beyond $10{\cdot}25$. By answering this question and resolving the paradox of the gap in the solutions, we shall gain considerable insight into the nature of similarity solutions and into the structure of many other flows as well.

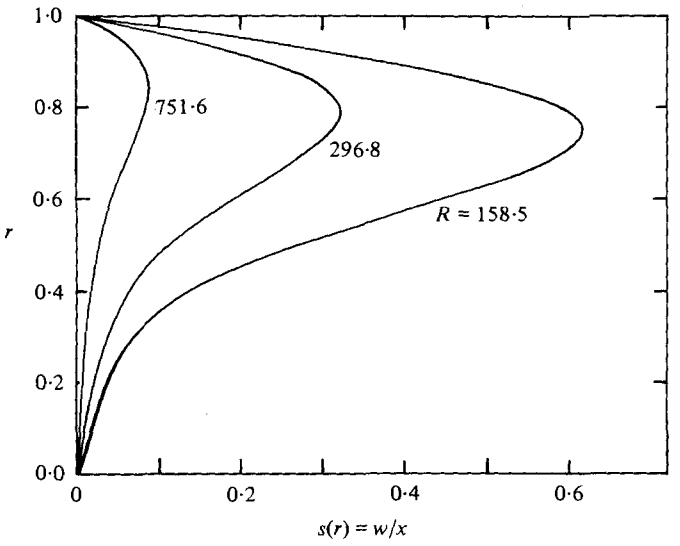

FIGURE 17. Group VI swirling velocity profiles at R = 751·6, 296·8 and 158·5 for the axisymmetric flow in a tube with swirl.

This work was supported in part by the National Science Foundation under Grant ENG 78-17613.

REFERENCES

BATCHELOR, G. K. 1967 *Introduction to Fluid Dynamics*, p. 290. Cambridge University Press.

BRADY, J. F. 1981 Inertial effects in closed cavity flows and their influence on drop breakup. Ph.D. thesis, Stanford University.

BRADY, J. F. & ACRIVOS, A. 1981*a* Closed cavity laminar flows at moderate Reynolds numbers. *J. Fluid Mech.* (to appear).

BRADY, J. F. & ACRIVOS, A. 1981*b* The deformation and breakup of a slender drop in extensional flow: inertial effects. *J. Fluid Mech.* (to appear).

CRANE, L. J. 1970 Flow past a stretching plane. *Z. angew. Math. Phys.* **21**, 645.

PROUDMAN, I. 1960 An example of steady laminar flow at large Reynolds number. *J. Fluid Mech.* **9**, 593.

ROBINSON, W. A. 1976 The existence of multiple solutions for the laminar flow in a uniformly porous channel with suction at both walls. *J. Eng. Math.* **10**, 23.

SECOMB, T. W. 1978 Flow in a channel with pulsating walls. *J. Fluid Mech.* **88**, 273.

SKALAK, F. M. & WANG, C.-Y. 1977 Pulsatile flow in a tube with injection and suction. *Appl. Sci. Res.* **33**, 269.

TERRILL, R. M. 1964 Laminar flow in a uniformly porous channel. *Aero. Quart.* **15**, 297.

TERRILL, R. M. 1965 Laminar flow in a uniformly porous channel with large injection. *Aero. Quart.* **16**, 323.

TERRILL, R. M. 1973 On some exponentially small terms arising in the flow through a porous pipe. *Quart. J. Appl. Math.* **26**, 347.

TERRILL, R. M. & THOMAS, P. W. 1969 On laminar flow through a uniformly porous pipe. *Appl. Sci. Res.* **21**, 37.

TERRILL, R. M. & THOMAS, P. W. 1973 Spiral flow in a porous pipe. *Phys. Fluids* **16**, 356.

VAN DYKE, M. 1974 Analysis and improvement of perturbation series. *Quart. J. Mech. Appl. Math.* **27**, 423.

VAN DYKE, M. 1975 *Perturbation Methods in Fluid Mechanics*, p. 89. Parabolic.

VAN DYKE, M. 1978 Extended Stokes series: laminar flow through a loosely coiled pipe. *J. Fluid Mech.* **86**, 129.